RADIO SCIENCE, VOL. 42, RS2006, doi:10.1029/2006RS003509, 2007

Scattering properties of electromagnetic waves in a multilayered cylinder filled with double negative and positive materials

Hai-Ying Yao,[1] Le-Wei Li,[1,2] Cheng-Wei Qiu,[1] Qun Wu,[3] and Zhi-Ning Chen[4,5]

Received 7 April 2006; revised 15 September 2006; accepted 7 November 2006; published 17 March 2007.

[1] In this paper, a multilayered cylinder filled with double negative (DNG) material and double positive (DPS) material is studied. General formulas of electromagnetic fields in each region are derived using the eigenfunction expansion method. The expansion coefficients are determined by a recursive system that is derived from boundary conditions at the multiple interfaces. The reflection by a cylinder with $(-\varepsilon_0, -\mu_0)$ (where ε_0 and μ_0 denote the permittivity and permeability in free space, respectively) is found to be quickly diminished with its electric size. For an infinite line source, the image property is observed when the radius of this cylinder is much larger than the wavelength. The distributions of electromagnetic fields are presented when a line source is placed near a two-layered cylinder alternately filled with DNG and DPS material. Numerical results confirm that the developed formulas are suitable to analyze the other multilayered cylindrical structures with DNG and DPS materials.

Citation: Yao, H. Y., L.-W. Li, C.-W. Qiu, Q. Wu, and Z.-N. Chen (2007), Scattering properties of electromagnetic waves in a multilayered cylinder filled with double negative and positive materials, *Radio Sci.*, *42*, RS2006, doi:10.1029/2006RS003509.

1. Introduction

[2] The permeability and permittivity of materials are two fundamental parameters of the constitutive relations which determine how the media interact with electromagnetic (EM) waves propagating in the materials. In 1968, *Veselago* [1968] theoretically studied wave characteristics in a special medium whose permittivity and permeability are both negative simultaneously. These hypothetical materials exhibit a left-handed rule defining the polarizations of electric and magnetic fields and the propagation vector constant and the media are thus referred to as left-handed materials (LHM) in literature [*Chen et al.*, 2004; *Grbic and Eleftheriades*, 2004; *Katsarakis et al.*, 2004; *Ziolkowski and Kipple*, 2003; *Panoiu and Osgood*, 2003; *Kuzmiak and Maradudin*, 2002; *Markos and Soukoulis*, 2002; *Yao et al.*, 2005a, 2005b]. The double negative (DNG) material has shown special optical properties, and could lead to a perfect lens [*Pendry*, 2000; *Zhang et al.*, 2002; *Pendry and Ramakrishna*, 2003; *Pendry*, 2003; *Ye*, 2003; *Ramakrishna and Pendry*, 2004].

[3] For EM waves propagating through a stratified DNG medium, reflection and refraction of the waves were formulated by *Kong* [2002]. The objective of this paper is to extend the existing application from planar structures to cylindrical structures, so as to gain more insight into the hybrid effects of metamaterials and cylindrical curvature. Potential applications of the results in this work include the conformal antenna radome analysis and design, two-dimensional microwave and optical imaging, etc. In this paper, we first derive a general formula of EM fields in all regions of a multilayered cylinder with DNG and DPS materials in this paper. The eigenfunction expansion method is applied to express the EM fields in this structure. To verify our formulations and validate our analysis, the distant scattering sections for a two-layered cylinder with double positive medium are first shown. Next, we consider some special cases to characterize the DNG materials. The first example that we consider is a dielectric cylinder with $(-\varepsilon_0, -\mu_0)$ which has a refractive index of $n = -1$. For

[1]Department of Electrical and Computer Engineering, National University of Singapore, Singapore.
[2]Also with Department of Electronics and Communications Engineering, Harbin Institute of Technology, Harbin, China.
[3]Department of Electronics and Communications Engineering, Harbin Institute of Technology, Harbin, China.
[4]Institute for Infocomm Research, Singapore.
[5]Also with Department of Electrical and Computer Engineering, National University of Singapore, Singapore.

0048-6604/07/2006RS003509$11.00

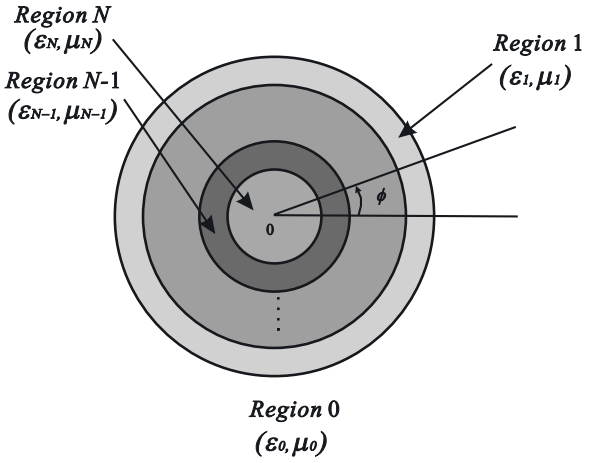

Figure 1. Geometry of a multilayered cylinder with different materials.

the incidence wave of transverse magnetic polarization, the reflection visibly diminishes when the electric size of the cylinder is increased. When a parallel line source is placed nearby, focus phenomenon is observed clearly inside the cylinder, provided that the electric size of the cylinder is much larger than the wavelength. Finally, distributions of field components are shown to confirm applicability of these formulas.

2. Formulations

[4] Consider an N-layered infinitely long cylinder situated in free space (ε_0, μ_0), as depicted in Figure 1. In each layer, it is filled with DNG or DPS homogeneous material of different permittivity and permeability. In the following analysis the time dependence, $e^{-j\omega t}$, is suppressed. The permittivity and permeability of material in region f ($f = 0,\ldots N$) are denoted as follows:

$$\varepsilon_f = u|\varepsilon_f| \tag{1}$$

$$\mu_f = u|\mu_f|, \tag{2}$$

where

$$u = \begin{cases} -1, & \text{DNG material} \\ 1, & \text{DPS material.} \end{cases} \tag{3}$$

[5] An incident wave of transverse electric (TE) or transverse magnetic (TM) polarization is assumed to illuminate the layered cylinder in free space at an arbitrary oblique angle. In the cylindrical coordinates system, the vector wave functions are given in [*Li et al.*, 2000], and rewritten as follows:

$$\mathbf{M}_n^{(p)}(k_z) = \left[\hat{\rho}\frac{jn}{\rho}B_n^{(p)}(k_\rho\rho) - \hat{\phi}\frac{dB_n^{(p)}(k_\rho\rho)}{d\rho}\right]e^{j(n\phi+k_z z)} \tag{4}$$

$$\mathbf{N}_n^{(p)}(k_z) = \frac{1}{k}\left[\hat{\rho}jk_z\frac{dB_n^{(p)}(k_\rho\rho)}{d\rho} - \hat{\phi}\frac{nk_z}{\rho}B_n^{(p)}(k_\rho\rho) + \hat{z}k_\rho^2 B_n^{(p)}(k_\rho\rho)\right]e^{j(n\phi+k_z z)}, \tag{5}$$

where $B_n^{(p)}(k_\rho\rho)$ represents the cylindrical Bessel functions of order n, the superscript p equals 1 or 3 representing the Bessel function of the first kind and the cylindrical Hankel function of the first kind, and $k^2 = k_\rho^2 + k_z^2$. If the electromagnetic waves are normally incident on the surface, the vector wave functions expressed in (4) and (5) can be simplified as

$$\mathbf{M}_n^{(p)}(k) = \left[\hat{\rho}\frac{jn}{\rho}B_n^{(p)}(k\rho) - \hat{\phi}\frac{dB_n^{(p)}(k\rho)}{d\rho}\right]e^{jn\phi} \tag{6}$$

$$\mathbf{N}_n^{(p)}(k) = \hat{z}kB_n^{(p)}(k\rho)e^{jn\phi}. \tag{7}$$

[6] By using eigenfunction expansion method, the electric and magnetic fields in the region f ($f = 1,\ldots N-1$) are formulated as follows:

$$\mathbf{E}_f = \sum_{n=0}^{\infty}\left\{a_{nf}\mathbf{N}_n^{(3)}(k_{zf}) + b_{nf}\mathbf{M}_n^{(3)}(k_{zf}) + a'_{nf}\mathbf{N}_n^{(1)}(k_{zf}) + b'_{nf}\mathbf{M}_n^{(1)}(k_{zf})\right\} \tag{8}$$

$$\mathbf{H}_f = \frac{k_f}{j\omega|\mu_f|}\sum_{n=0}^{\infty}\left\{a_{nf}\mathbf{M}_n^{(3)}(k_{zf}) + b_{nf}\mathbf{N}_n^{(3)}(k_{zf}) + a'_{nf}\mathbf{M}_n^{(1)}(k_{zf}) + b'_{nf}\mathbf{N}_n^{(1)}(k_{zf})\right\}, \tag{9}$$

where a_{nf}, b_{nf}, a'_{nf} and b'_{nf} are the unknown expansion coefficients.

[7] For the outmost region (i.e., Region 0) and the innermost region (i.e., Region N), the electromagnetic fields can be expanded as

$$\mathbf{E}_0 = \mathbf{E}^i + \mathbf{E}^s = \mathbf{E}^i + \sum_{n=0}^{\infty}\left[a_{n0}\mathbf{N}_n^{(3)}(k_{z0}) + b_{n0}\mathbf{M}_n^{(3)}(k_{z0})\right] \tag{10}$$

$$\mathbf{H}_0 = \mathbf{H}^i + \mathbf{H}^s = \mathbf{H}^i + \frac{k_0}{j\omega u|\mu_0|} \times \sum_{n=0}^{\infty} \left[a_{n0}\mathbf{M}_n^{(3)}(k_{z0}) + b_{n0}\mathbf{N}_n^{(3)}(k_{z0}) \right] \tag{11}$$

and

$$\mathbf{E}_N = \sum_{n=0}^{\infty} \left[a'_{nN}\mathbf{N}_n^{(1)}(k_{zN}) + b'_{nN}\mathbf{M}_n^{(1)}(k_{zN}) \right] \tag{12}$$

$$\mathbf{H}_N = \frac{k_N}{j\omega u|\mu_N|} \sum_{n=0}^{\infty} \left[a'_{nN}\mathbf{M}_n^{(1)}(k_{zN}) + b'_{nN}\mathbf{N}_n^{(1)}(k_{zN}) \right]. \tag{13}$$

For the electromagnetic fields in all the regions, we have the same longitudinal wave vector k_z because of the phase matching condition, whereas the radial wave vector $k_{\rho f}$ is discontinuous.

[8] In the above formulas, the expansion coefficients, a_{nf}, b_{nf}, a'_{nf}, and b'_{nf}, can be determined by enforcing the boundary conditions of the tangential electric and magnetic field components on the cylindrical interfaces at $\rho = r_f$ (where $f = 0,1,\ldots, N-1$):

$$\hat{\rho} \times \begin{bmatrix} \mathbf{E}_f \\ \mathbf{H}_f \end{bmatrix} = \hat{\rho} \times \begin{bmatrix} \mathbf{E}_{f+1} \\ \mathbf{H}_{f+1} \end{bmatrix}. \tag{14}$$

A recursive system for the coefficients can be finally obtained [*Li et al.*, 2000]:

$$C_{f+1} = \mathbf{T}_f C_f, \tag{15}$$

where $[C_f]$ is defined by

$$C_f = \left[a_{nf},\ b_{nf},\ a'_{nf},\ b'_{nf} \right]^T, \tag{16}$$

the transmission matrix in the eigenexpansion domain is given by

$$\mathbf{T}_f = \mathbf{F}_{f+1}^{-1}\mathbf{F}_f, \tag{17}$$

and the parameter matrices $\mathbf{F}_f$ and $\mathbf{F}_{f+1}$ are derived from the boundary conditions.

[9] Employing the coefficients in the region 0 and the Nth region, the scattering coefficients, a_{n0} and b_{n0}, can be derived. With the known a_{n0}, b_{n0}, a'_{n0}, and b'_{n0} in region 0, the scattering coefficients, a_{nf}, b_{nf}, a'_{nf}, and b'_{nf} in region f can be determined by the recursive relationship as in equation (15). Hence the total electric and magnetic fields in any region can be found.

2.1. Incident TE_z and TM_z Waves

[10] The incident TE_z and TM_z waves, which are expanded in terms of $\mathbf{M}_n$ and $\mathbf{N}_n$, have the following forms:
for the TM wave,

$$\mathbf{E}_{TM}^i = \frac{E_0^{TM}}{k\sin\theta_0} \sum_{n=0}^{\infty} (2-\delta_{n0}) j^n \mathbf{N}_n^{(1)}(k_z) e^{-jn\phi_0} \tag{18}$$

$$\mathbf{H}_{TM}^i = \frac{E_0^{TM}}{j\eta_0 k\sin\theta_0} \sum_{n=0}^{\infty} (2-\delta_{n0}) j^n \mathbf{M}_n^{(1)}(k_z) e^{-jn\phi_0}, \tag{19}$$

and for the TE wave,

$$\mathbf{E}_{TE}^i = \frac{E_0^{TE}}{jk\sin\theta_0} \sum_{n=0}^{\infty} (2-\delta_{n0}) j^n \mathbf{M}_n^{(1)}(k_z) e^{-jn\phi_0} \tag{20}$$

$$\mathbf{H}_{TE}^i = -\frac{E_0^{TE}}{\eta_0 k\sin\theta_0} \sum_{n=0}^{\infty} (2-\delta_{n0}) j^n \mathbf{N}_n^{(1)}(k_z) e^{-jn\phi_0}, \tag{21}$$

where $\delta_{mn} = 1$ for $m = n$; or 0 for $m \neq n$ while the vector wave functions $\mathbf{M}$ and $\mathbf{N}$ are denoted by equations (4) and (5).

[11] Thus a'_{n0} and b'_{n0} are represented by

$$a'_{n0} = (2-\delta_{n0}) j^n \frac{E_0^{TM}}{k_0\sin\theta_0} e^{-jn\phi_0} \tag{22}$$

$$b'_{n0} = -(2-\delta_{n0}) j^{n+1} \frac{E_0^{TE}}{k_0\sin\theta_0} e^{-jn\phi_0}. \tag{23}$$

The parameter matrix $\mathbf{F}_f$, where $\rho = r_f$, can be obtained:

$$\mathbf{F}_f = -\begin{bmatrix} \frac{nk_z}{k_f\rho} H_n^{(1)}(k_{\rho f}\rho) & \frac{dH_n^{(1)}(k_{\rho f}\rho)}{d\rho} & \frac{nk_z}{k_f\rho} J_n(k_{\rho f}\rho) & \frac{dJ_n(k_{\rho f}\rho)}{d\rho} \\ \frac{k_{\rho f}^2}{k_f} H_n^{(1)}(k_{\rho f}\rho) & 0 & \frac{k_{\rho f}^2}{k_f} J_n(k_{\rho f}\rho) & 0 \\ \frac{k_f}{j\omega u|\mu_f|} \frac{dH_n^{(1)}(k_{\rho f}\rho)}{d\rho} & \frac{nk_z}{j\omega u|\mu_f|\rho} H_n^{(1)}(k_{\rho f}\rho) & \frac{k_f}{j\omega u|\mu_f|} \frac{dJ_n(k_{\rho f}\rho)}{d\rho} & \frac{nk_z}{j\omega u|\mu_f|\rho} J_n(k_{\rho f}\rho) \\ 0 & \frac{k_{\rho f}^2}{j\omega u|\mu_f|} H_n^{(1)}(k_{\rho f}\rho) & 0 & \frac{k_{\rho f}^2}{j\omega u|\mu_f|} J_n(k_{\rho f}\rho) \end{bmatrix}. \tag{24}$$

2.2. Infinitely Long Line Source

[12] For an infinitely long line source placed at (ρ_0,ϕ_0) and parallel to the cylinder, the incident electromagnetic wave can be expressed by

$$\mathbf{E}^i = -\frac{k^2 I}{4\omega\varepsilon_0}\sum_{n=0}^{\infty}(2-\delta_{n0})H_n^{(1)}(k\rho_0)\mathbf{N}_n^{(1)}(k)e^{-jn\phi_0} \quad (25)$$

$$\mathbf{H}^i = -\frac{kI}{4j}\sum_{n=0}^{\infty}(2-\delta_{n0})H_n^{(1)}(k\rho_0)\mathbf{M}_n^{(1)}(k)e^{-jn\phi_0}, \quad (26)$$

where I stands for the amplitude of electric current, ρ_0 denotes the distance from the center of cylinder, and the vector wave functions **M** and **N** are denoted by equations (6) and (7).

[13] Then, a'_{n0} and b'_{n0} are represented by

$$a'_{n0} = -(2-\delta_{n0})\frac{k_0^2 I}{4\omega\varepsilon_0}H_n^{(1)}(k_0\rho_0)e^{-jn\phi_0} \quad (27)$$

$$b'_{n0} = 0. \quad (28)$$

Similarly, $\mathbf{F}_f$, where $\rho = r_f$, can be derived:

$$\mathbf{F}_f = -\begin{bmatrix} 0 & \frac{dH_n^{(1)}(k_f\rho)}{k_f d\rho} & 0 & \frac{dJ_n(k_f\rho)}{k_f d\rho} \\ H_n^{(1)}(k_f\rho) & 0 & J_n(k_f\rho) & 0 \\ \frac{k_f}{j\omega u|\mu_f|}\frac{dH_n^{(1)}(k_f\rho)}{k_f d\rho} & 0 & \frac{k_f}{j\omega u|\mu_f|}\frac{dJ_n(k_f\rho)}{k_f d\rho} & 0 \\ 0 & \frac{k_f}{j\omega u|\mu_f|}H_n^{(1)}(k_f\rho) & 0 & \frac{k_f}{j\omega u|\mu_f|}J_n(k_f\rho) \end{bmatrix}. \quad (29)$$

3. Numerical Results

[14] To verify the correctness of the formulations deduced above, we first calculate the distant scattering pattern of a two-layered (three regions) cylinder filled with different DPS materials and illuminated by the TE and TM waves, and radiated by the parallel line source, respectively. The geometry is shown in Figure 2. The radii of two layers from inside to outside are $a = 0.25\lambda$ and $b = 0.3\lambda$, respectively. The corresponding relative permittivity are $\varepsilon_{r1} = 4.0$, and $\varepsilon_{r2} = 1.0$. The relative permeability of two layers are $\mu_{r1} = \mu_{r2} = 1.0$. The plane waves are assumed to be at normal incidence. The line source is placed at a distance of $\rho_0 = 0.5\lambda$ from the center of the layered cylinder, and an observation angle ϕ_0 of 0 degree. The distant scattering pattern can be obtained by the asymptotic form of large-argument Hankel functions. The results are shown in Figures 3 and 4, respectively. For the reference, the integral equation solutions, which come from *Richmond* [1965, 1966], are also given. An excellent agreement is observed between the existing solution presented by *Richmond* [1965, 1966] and those that we newly obtain. This partially verified the correctness of our derived theoretical formulas and the developed codes.

[15] Subsequently, we utilize these formulas to calculate the electromagnetic fields in the presence of the multilayered cylinder filled with DNG and DPS materials. In order to illustrate better the usefulness of these general formulas, the constitutive parameters of DNG materials are specified by $(-\varepsilon_0, -\mu_0)$ and those of DPS materials are (ε_0, μ_0) in the following computations. The cylindrical interfaces are all depicted by circular curves in the figures.

[16] First of all, the normalized scattering cross section σ/λ of a one-layered (two regions) cylinder filled with DNG $(-\varepsilon_0, -\mu_0)$ material is calculated under illumination by the incident TM wave with the angles of $\theta^i = \pi/2$ and $\phi^i = \pi$ in the free space. Curves for different radii a of the cylinder are plotted in Figure 5. It is obvious that the reflection by the cylinder is quickly diminished with the increase of the radius. We can also observe that the RCS data at and near $\phi = 0^\circ$ are very large and it is of the impulse shape when the cylindrical radius is large. This phenomenon can be explained as follows.

[17] 1. Intensity: First of all, in Figure 5, the incident wave (a TM-polarized plane wave) is impinged at an angle of elevation $\theta^i = 90^\circ$ and azimuth $\phi = 180^\circ$. In this case, some portion of the wave energy is normally incident upon the cylinder, so the transmitted wave due to this portion propagates entirely through the dielectric cylinder when the impedance is matched ($\varepsilon_r = \mu_r = -1$). This portion of waves contributes to part of bistatic RCS datum of $\phi = 0^\circ$. For a cylinder of large radius, illumination area by normal or nearly normal incident waves is larger than that of a cylinder of smaller radius. In this case, the cylinder tends to be a perfectly matched layer and it is almost transparent to the incident wave (especially when the wave is forward propagating). Therefore the percentage of the energy propagated through the cylinder will be relatively larger.

[18] 2. Beam width: Secondly, the cylinder behaves as a dielectric lens. For RCS computations, we take the observation point at infinity. When the incident wave propagates through the cylinder filled with DNG, the focus point will approach to infinity because of the

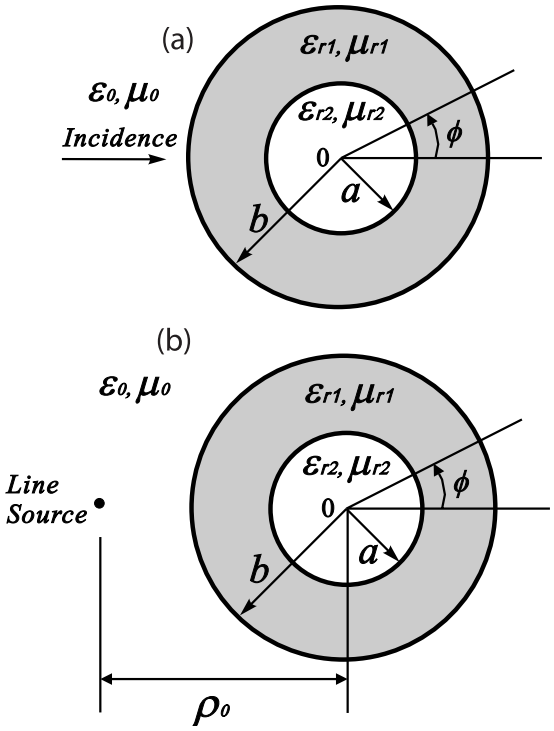

Figure 2. Geometry of a two-layered cylinder with DPS materials.

smoother dielectric curvature. For example, when ka = 100, the observation point (infinity) lies to the right of the focus point (which is already sufficiently far away from origin). Thus it can be imagined that the angle of coverage is small at around $\phi = 0°$. When the radius becomes larger and larger, the observation point and the focus point will move closer and closer to each other. In an extreme case, when the cylinder tends to approach a flat slab, the angle of coverage is almost zero to form a delta.

[19] That is why the scattering cross sections around the angle of $\phi = 0°$ are thus much stronger, but confined within a very narrow angle.

[20] Then, radiation by a line source in the presence of this cylinder is considered. The different radii for a

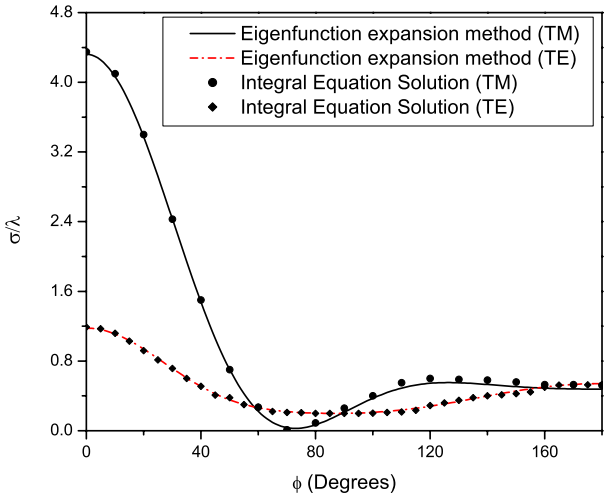

Figure 3. Distant scattering pattern of TE and TM waves illuminating a two-layered cylinder with DPS materials.

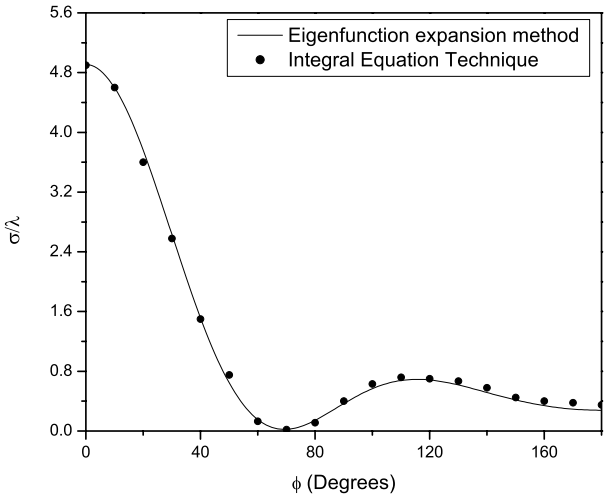

Figure 4. Scattering pattern of a nearby parallel line source in the presence of a two-layered cylinder with DPS materials.

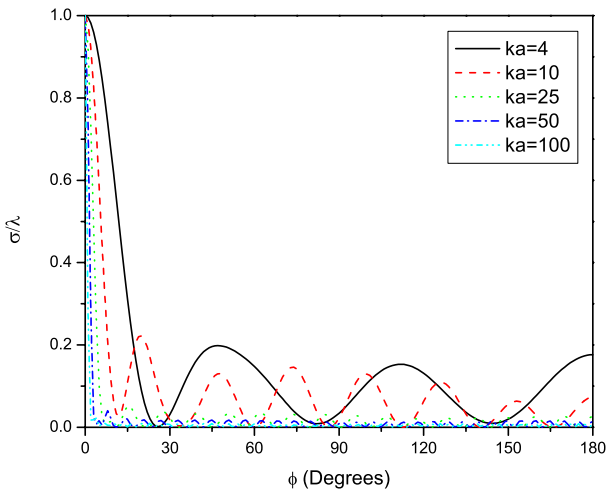

Figure 5. Normalized scattering cross section of a one-layered cylinder of different radii and with $(-\varepsilon_0, -\mu_0)$.

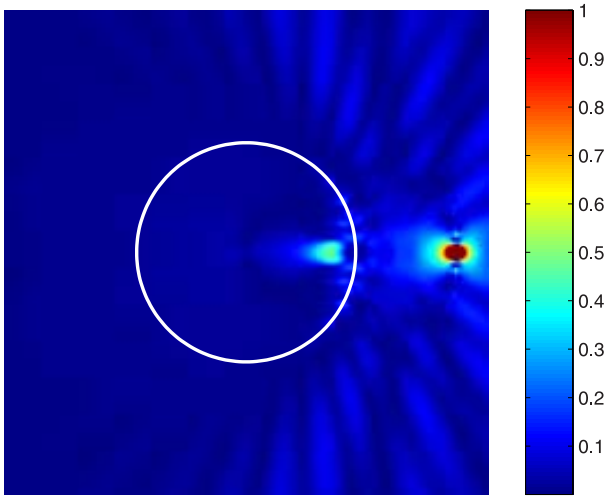

Figure 6. Normalized amplitudes of the time-averaged Poynting power for a one-layered cylinder with $(-\varepsilon_0, -\mu_0)$ and $a = 2.5\lambda$.

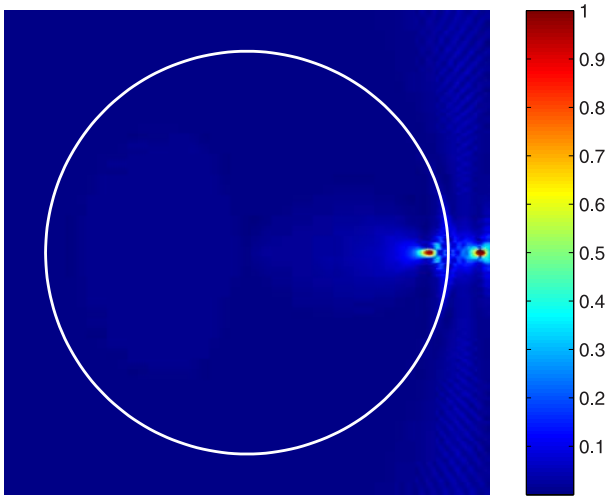

Figure 8. Normalized amplitudes of the time-averaged Poynting power for a one-layered cylinder with $(-\varepsilon_0, -\mu_0)$ and $a = 150\lambda$.

values are also set. The line source is located at $\rho_1 = 2.3\lambda$ and $\phi_0 = 0$, where ρ_1 is the distance from the surface of the cylinder. The normalized amplitudes of the time-averaged Poynting power, which is denoted by $\langle \mathbf{S} \rangle = \frac{1}{2}\mathbf{Re}(\mathbf{E} \times \mathbf{H}^*)$, are shown in Figures 6, 7, and 8. From Figures 6 and 7, we observe that a facula is formed inside the cylinder. The formation of the facula is due to the cylinder with $(-\varepsilon_0, -\mu_0)$ is not a focusing system. This summary point can be verified by using the theory of arbitrary coordinate transformations [*Ward and Pendry*, 1996]. According to the theory, if we keep the wave scattering properties unchanged after the geometrical dimension (e.g., the radius) is changed, we have to adjust μ and ε accordingly. When the physical problem is changed from a perfect slab lens to a perfect cylindrical lens, the permittivity and permeability in the lens are required to be a function of position. Hence the cylinder with $(-\varepsilon_0, -\mu_0)$ cannot focus the light, and it will still reflect waves. However, a phenomenon of focus shown as in Figure 8 and very small reflection shown as in Figure 5 can be obtained when the electric size of calculated problem is far larger than the wavelength.

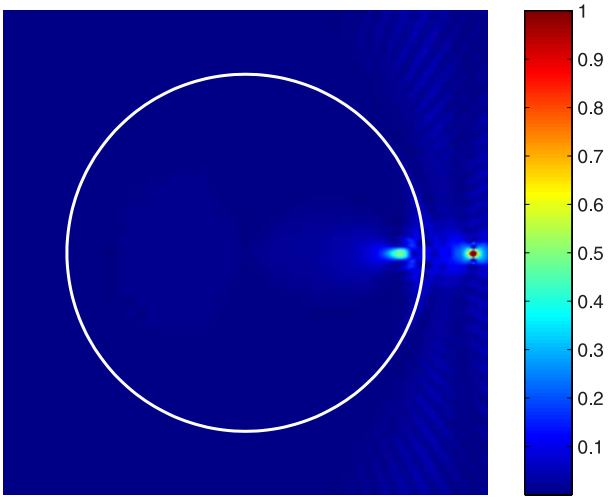

Figure 7. Normalized amplitudes of the time-averaged Poynting power for a one-layered cylinder with $(-\varepsilon_0, -\mu_0)$ and $a = 8.5\lambda$.

[21] Finally, the real parts of field components, H_ρ, H_ϕ and E_z, scattered by a two-layered (three regions) cylinder filled alternately with DNG and DPS material are shown in Figures 9, 10, and 11. In this case, a line source is placed at $\rho_0 = 9.5\lambda$ and $\phi_0 = 0$, the radii of two layers are $r_1 = 8\lambda$ and $r_2 = 5\lambda$, respectively. The region 0 is the free space, region 1 and 2 are filled with $(-\varepsilon_0, -\mu_0)$ and (ε_0, μ_0) respectively. As we expect, the tangential components H_ϕ and E_z are equal on the layered interfaces. While the normal component H_ρ is not, which satisfies by default the continuity of normal component of magnetic flux density **B** across the interfaces between the DNG and DPS materials.

4. Conclusion

[22] In this paper, we applied the eigenfunction expansion method to generally express the fields in a multilayered cylinder filled by a double negative medium and a double positive medium. The eigenfunction expansion

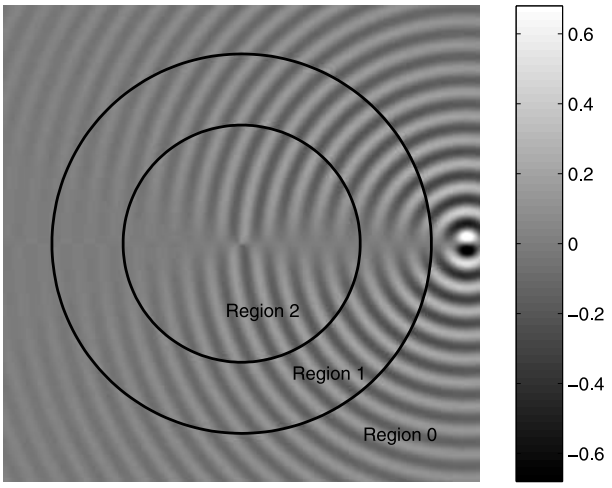

Figure 9. Real part of the H_ρ component of an electromagnetic wave propagating through a two-layered cylinder with DNG and DPS materials.

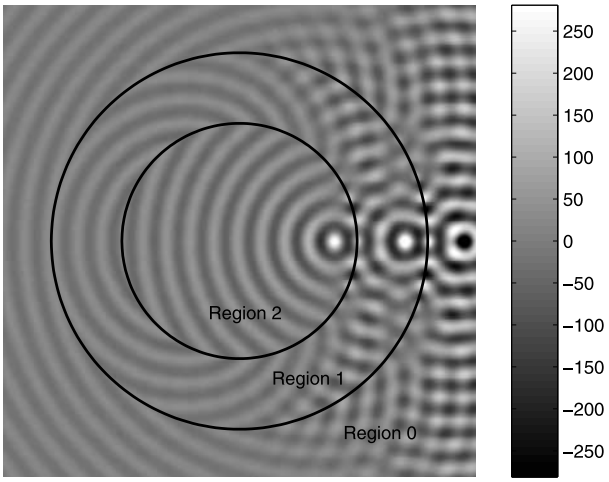

Figure 11. Real part of the E_z component of an electromagnetic wave propagating through a two-layered cylinder with DNG and DPS materials.

coefficients are determined by enforcing the tangential electric and magnetic field components continuous at the interfaces. By applying the asymptotic form of large-argument Hankel functions, the distant or far-zone scattering patterns for a one-layered cylinder with left($-\varepsilon_0$, $-\mu_0$) and different radii are obtained. The results show that the reflection is vanished with the increasing radius. Moreover, the imaging of a line source by this cylinder is observed when the radius $r \gg \lambda$. Finally, field components for a two-layered cylinder alternately filled with DNG and DPS materials are calculated. The normal component is found to be discontinuous at the boundaries, and the tangential components are not, which agrees, as expected, with the boundary conditions.

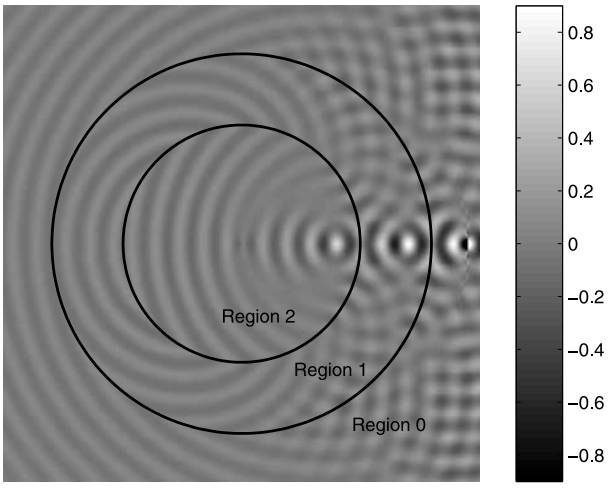

Figure 10. Real part of the H_ϕ component of an electromagnetic wave propagating through a two-layered cylinder with DNG and DPS materials.

[23] **Acknowledgments.** The authors are grateful to the financial support in terms of a research grant (WBS: R-263-000-340-592) from the Singaporean Agency for Science, Technology, and Research (A-STAR) via the Institute of Infocomm Research (I2R); to the support from SUMMA Foundation, United States, in terms of a SUMMA Graduate Fellowship; to the Joint Program offered by the National University of Singapore (in Singapore) and Supelec (in Paris, France) in terms of the financial support by both parties; to the support by a U.S. Air Force Project (AOARD-064031); and to the joint project supported by the France-Singapore "Merlion Project."

References

Chen, H. S., L. X. Ran, J. T. Huangfu, X. M. Zhang, K. S. Chen, T. M. Grzegorczyk, and J. A. Kong (2004), Left-handed materials composed of only S-shaped resonators, *Phys. Rev. E*, *70*, 057605.

Grbic, A., and G. V. Eleftheriades (2004), Overcoming the diffraction limit with a planar left-handed transmission-line lens, *Phys. Rev. Lett.*, *92*, 117403.

Katsarakis, N., T. Koschny, M. Kafesaki, E. N. Economou, E. Ozbay, and C. M. Soukoulis (2004), Left- and right-handed transmission peaks near the magnetic resonance frequency in composite metamaterials, *Phys. Rev. B*, *70*, 201101.

Kong, J. A. (2002), Electromagnetic wave interaction with stratified negative isotropic media, *Prog. Electromagn. Res.*, *35*, 1–52.

Kuzmiak, V., and A. A. Maradudin (2002), Scattering proprtties of a cylinder fabricated from a left-handed material, *Phys. Rev. B*, *66*, 045116.

Li, L. W., D. You, M. S. Leong, and T. S. Yeo (2000), Electromagnetic scattering by multilayered chiral-media structures: A scattering-to-radiation transform, *Prog. Electromagn. Res.*, *26*, 249–291.

Markos, P., and C. M. Soukoulis (2002), Numerical studies of left-handed materials and arrays of split ring resonators, *Phys. Rev. E.*, *65*, 036622.

Panoiu, N. C., and R. M. Osgood (2003), Influence of the dispersive properties of metals on the transmission characteristics of left-handed materials, *Phys. Rev. E*, *68*, 016611.

Pendry, J. B. (2000), Negative refraction makes a perfect lens, *Phys. Rev. Lett.*, *85*, 3966–3969.

Pendry, J. B. (2003), Perfect cylindrical lenses, *Optics Express*, *11*(7), 755–760.

Pendry, J. B., and S. A. Ramakrishna (2003), Focusing light using negative refraction, *Z. Phys. B. Condens. Matter*, *15*, 6345–6364.

Ramakrishna, S. A., and J. B. Pendry (2004), Spherical perfect lens: Solutions of Maxwell's equations for spherical geometry, *Phys. Rev. B*, *69*, 115115.

Richmond, J. R. (1965), Scattering by a dielectric cylinder of arbitrary cross-section shape, *IEEE Trans. Antennas Propag.*, *13*(3), 334–341.

Richmond, J. R. (1966), TE-wave scattering by a dielectric cylinder of arbitrary cross-section shape, *IEEE Trans. Antennas Propag.*, *14*(4), 460–464.

Veselago, V. G. (1968), The electrodynamics of substances with simultaneously negative values of ε and μ, *Sov. Phys. Usp.*, Engl. Transl., *10*(4), 509–514.

Ward, A. J., and J. B. Pendry (1996), Refraction and geometry in Maxwell's equation, *J. Mod. Optics*, *43*(4), 773–793.

Yao, H. Y., L. W. Li, Q. Wu, and J. A. Kong (2005a), Macroscopic performance analysis of metamaterials synthesized from microscopic 2-D isotropic cross split-ring resonator array, *Prog. Electromagn. Res.*, *51*, 197–217.

Yao, H. Y., W. Xu, L. W. Li, Q. Wu, and T. S. Yeo (2005b), Propagation property analysis of metamaterial constructed by conductive SRRs and wires using the MGS-based algorithm, *IEEE Trans. Microwave Theory Tech.*, *53*(4), 1469–1476.

Ye, Z. (2003), Optical transmission and reflection of perfect lenses by left handed materials, *Phys. Rev. B*, *67*, 193106.

Zhang, Y., T. M. Grzegorczyk, and J. A. Kong (2002), Propagation of electromagnetic waves in a slab with negative permittivity and negative permeability, *Prog. Electromagn. Res.*, *35*, 271–286.

Ziolkowski, R. W., and A. D. Kipple (2003), Causality and double-negative metamaterials, *Phys. Rev. E*, *68*, 026615.

Z. N. Chen, Institute for Infocomm Research, 20 Science Park Road, 02-34/37 TeleTech Park, Singapore 117674. (chenzn@i2r.a-star.edu.sg)

L. W. Li, C. W. Qiu, and H. Y. Yao, Department of Electrical and Computer Engineering, National University of Singapore, 10 Kent Ridge Crescent, Singapore 119260. (lwli@nus.edu.sg; g0305774@nus.edu.sg; eleyh@nus.edu.sg)

Q. Wu, Department of Electronics and Communications Engineering, Harbin Institute of Technology, 92 Xidazhi Street, Harbin 150001, China. (qwu@hit.edu.cn)